CrystEngComm

ROYAL SOCIETY OF CHEMISTRY

PAPER

View Article Online
View Journal

Cite this: DOI: 10.1039/d6ce00109b

Solid–liquid equilibria in the aqueous chiral homophenylalanine system and solid-state characterisation of the racemic species

Axel Schultheis,[a] Klaus Merz,[b] Vico Tenberg[ac] and Heike Lorenz *[a]

Received 5th February 2026,
Accepted 19th March 2026

DOI: 10.1039/d6ce00109b

rsc.li/crystengcomm

In this work, solid–liquid equilibria of the ternary system D-HPA/L-HPA/water were investigated at 25 and 55 °C. The chiral system is of the racemic compound forming type and characterised by very low solubilities below 0.2 wt% at 55 °C. The solid state behaviour of DL-HPA was analysed employing differential scanning calorimetry and hot stage microscopy showing a decomposition behaviour at elevated temperatures *i.e.* no melting point. Exemplary for the chiral system, milled samples of L-HPA were studied by powder X-ray diffractometry confirming the tendency of the crystals to preferred orientation. For the first time, single crystal structures of L-HPA and DL-HPA were determined, and deposited in the CCDC (2463661–2463662). No further solid-state forms were encountered in the temperature and solvent condition range studied. Comparison to the chiral phenylalanine system revealed similar thermal behaviour and solubility relationships except the strong difference in absolute solubilities.

1 Introduction

Amino acids are substances relevant in nature, medicine, food, and pharmaceutical industries amongst others.[1] They are chiral compounds and therefore appear in L- and D-configurations[2] potentially with varying (bio-)chemical properties of the enantiomers.[2,3] One enantiomer might show desired properties, *e.g.* as an active pharmaceutical ingredient, while the other is not effective or may even be harmful.[2] This emphasises the need for enantiopure products, which might originate from an enantioselective synthesis. The respective substance must then be isolated, *e.g.* in solid form, by crystallisation. If the synthesis is not completely enantioselective, the obtained substance must additionally be purified with regard to the desired enantiomer. The fundamentals for rigorous crystallization process design are the solvent choice, the corresponding solid–liquid equilibria (SLE) with the desired product, potentially contained impurities, and required process conditions.[2] For chiral amino acid systems, three basic solid-state behaviours are known: a) conglomerate forming systems, where the L- and D-form crystallise in separate crystals and the respective separate solid phases are mechanically mixed, b) racemic compound forming systems in which the L- and D-amino acids form a joined crystal lattice in a 1 : 1 ratio called racemate or racemic compound, and c) solid solution forming systems, where both molecules are statistically distributed within a single solid phase over a specific composition range.[2,4] The type of solid phase behaviour has tremendous influence on the appropriate separation strategies which can be coupled with deracemisation processes to increase the single-enantiomer yield.[2,5,6] Depending on the present SLE, the target and initial enantiomer composition, different crystallisation techniques can be employed for purification of the target enantiomer or yield increase *e.g.* "classical" enantioselective crystallisation or preferential crystallisation.[6]

This work focusses on the non-proteinogenic amino acid homophenylalanine (HPA), where the L-form is relevant in pharmaceutical applications as building block, intermediate, or precursor for novel pharmaceuticals including inhibitors or antibiotics.[7,8] Synthesis methods, especially biocatalytic pathways with good chiral purity, were investigated in literature.[7–10] The solubility-temperature relationship of L-HPA was investigated in ref. 9. This data was expanded by pH dependent SLE and various thermochemical properties of pure L-HPA in prior work of our group.[11] To the best of our knowledge, there is no such information for D-HPA or racemic DL-HPA in open literature merely the synthesis of racemic DL-HPA and its melting temperature is described.[12] Additionally, melting temperatures are also reported in respective safety data sheets.[13–15]

This work aims to provide fundamental SLE data in the chiral aqueous L-HPA/D-HPA system to enable selection of an appropriate crystallization-based purification method. Further, the solid-state behaviour of racemic DL-HPA was investigated

[a] *Max Planck Institute for Dynamics of Complex Technical Systems, Sandtorstrasse 1, 39106 Magdeburg, Germany. E-mail: lorenz@mpi-magdeburg.mpg.de*
[b] *Ruhr-Universität Bochum, Universitätsstr. 150, 44801 Bochum, Germany*
[c] *Otto von Guericke University, Universitätsplatz 2, 39106 Magdeburg, Germany*

Table 1 Details regarding the chemicals used in this work

Chemical	CAS	Supplier	Grade	M (g mol^{-1})
L-HPA	943-73-7	Thermo Fisher	98%	179.22
D-HPA	82795-51-5	Bld Pharmatech	98%	179.22
DL-HPA	1012-05-1	TCI	>97.0%	179.22
Water			Deionised	18.02
1 mol L^{-1} NaOH	1310-73-2	Merck Supelco	Titripur	40.00
Methanol	67-56-1	Merck Supelco	Liquid chromatography	32.04
Ammonium acetate	631-61-8	Sigma Life Science	Molecular biology	77.08
Acetic acid glacial	64-19-7	Fisher Scientific	HPLC grade	60.05

employing differential scanning calorimetry (DSC), hot stage microscopy (HSM), powder X-ray diffraction (PXRD). Additionally, single-crystal X-ray analysis (SC-XRD) was performed for the L-enantiomer and the racemic compound and, for the first time, crystal structures were determined.

2 Materials and methods

2.1 Materials

Chemicals used in this work will be introduced in this section and Table 1 summarises employed chemicals with CAS no., supplier, and grade. Substances were used as received, unless stated otherwise. For some experiments, HPA was refined by recrystallisation from water. Water was purified using a Milli-Q Advantage (Merck, Germany) to a total organic carbon content of 4 ppb and electric resistivity of 18.2 MΩ cm at 25 °C.

2.2 Solid–liquid equilibria (SLE) in the D-HPA/L-HPA/water system

An isothermal method was used to investigate the SLE in the system L-HPA/D-HPA/water. L-HPA/D-HPA/water or L-HPA/DL-HPA/water mixtures were prepared in varying compositions with a solid content up to 0.3 wt%. The resulting suspensions were brought to elevated temperature while being stirred on a heating plate to dissolve all solids. After apparent dissolution, the samples were equilibrated at target temperatures in a temperature controlled double-jacketed vessel for at least 7 days while getting continuously stirred. In a previous work,[11] we noticed that solid L-HPA accumulates on the liquid/air interface and at the bottom of the vial. To receive solid-free liquid samples for analyses, the magnetic stirring was deactivated several minutes prior to sampling and disposable syringe filters (pore size: 0.45 μm) were used. To obtain related solid samples, vacuum filtration was performed and some solid samples were washed with ethanol on employed glass frits (pore size: 10–16 μm). Liquid samples were analysed *via* HPLC, the solid phase identity was verified by PXRD either directly or after vacuum drying at 250 mbar at 40 °C. Solid compositions were measured by dissolving small amounts of the respective samples in the employed HPLC eluent followed by HPLC analysis.

We took great care to ensure total dissolution of added solids but the extraordinary low solubilities in the aqueous HPA system renders the dissolution process time consuming and unnoticed minuscule crystals might remained in the solution prior to equilibration. These could act as seed crystals favouring growth of the present solid phase instead of nucleation of the thermodynamically stable phase. To identify the thermodynamically stable solid phase, a similar set of experiments was performed where L-HPA and D-HPA in a 1 : 1 mass ratio or pure DL-HPA with a solid content of 0.1 wt% were dissolved by heating. The selected concentration corresponds approximately to the measured solubility of DL-HPA at 55 °C ensuring complete dissolution in equilibrium. Resulting liquid was filtered with a preheated glass frit (pore size: 10–16 μm), heated to 65 °C and maintained at this temperature for 2 h to dissolve minuscule crystals which might passed the filter. The respective thermostat was then switched to 25 °C guaranteeing a slow cooling curve instead of a crash cooling. The samples were equilibrated for 11 days at 25 °C and sampled for liquid and solid analysis, as described above.

The solubility of DL-HPA was determined by the same method as the ternary SLE with slight changes. Here only DL-HPA with a solid content of approximately 0.2 wt% was mixed with water and equilibrated at target temperatures for at least 6 days. The remaining steps were identical.

2.3 Milling experiments

Our initially measured PXRD patterns of L-HPA did not align well with the calculated pattern from the structure determination. To check whether the discrepancy originates from preferred orientation of the plate-like crystals or from a different solid form, we performed milling experiments decreasing the particle size and influencing particle morphology. These experiments were performed employing a ball mill MM 400 (Retsch, Germany). Used milling jars had a volume of 10 mL, were made of 1.4112 stainless steel and filled with three milling balls of 0.7 mm diameter of the same material. A milling frequency of 25 Hz was selected and in all experiments approximately 0.5 g recrystallised L-HPA were employed. Three types of conditions were tested to investigate the influence of mass and energy transfer:

- Dry grinding: base case.
- Wet grinding with 50 μL water: increased energy transfer due to the added liquid.
- Wet grinding with 50 μL 1 mol L^{-1} NaOH: increased energy transfer due the added liquid and additionally increased mass transfer as a result of elevated solubility.[16]

After specific times, the mill was stopped, samples for PXRD were taken and the milling was continued.

2.4 Analytical methods

High pressure liquid chromatography. Quantification of L-HPA and D-HPA was either performed in a UltiMate 3000 (Dionex Softron GmbH – Part of Thermo Fisher Scientific Inc, Germany) or an 1260 Infinity (Agilent, USA) depending on availability. The employed HPLC method[17,18] relies on usage of an Astec Chirobiotic T column (Sigma-Aldrich Chemie GmbH, Germany, 250 × 4.6 mm, particle size: 5 μm). The isocratic flow of 0.5 mL min^{-1} was composed of a volumetric mixture (70) : (30) (methanol) : (0.01 mol L^{-1} ammonium acetate + 0.5 mL L^{-1} acetic acid + water) mixture. The Injection volume was 10 μL or 100 μL depending on sample concentration. The column temperature was 23 °C (Agilent 1260 Infinity) or 25 °C (UltiMate 3000). In both devices, evaluation was performed by UV absorption at 210 nm. Retention times were approximately 9 min for L-HPA and 15 min for D-HPA (Agilent 1260 Infinity) or 21 min for L-HPA and 28 min for D-HPA (UltiMate 3000). Calibration was done by dissolving known amounts of L-HPA and D-HPA in the eluent and linear correlation of the measured area to the known composition. Employed calibrations were validated by analysis of samples with known concentration alongside samples from experiments.

Powder X-ray diffraction. Solid phase identification *via* powder X-ray diffractometry was performed using an X'Pert Pro diffractometer (PANalytical, The Netherlands) with CuKα radiation. Measurement was conducted in a 2θ range from 3 to 40°, with a counting time of 50 s and a step size of 0.017° at ambient conditions. For clear illustration, only 2θ from 6 to 30° are shown and the diffraction peaks were normalized to the maximal intensity of the respective measurement.

Single-crystal XRD analysis. Samples for single-crystal XRD analysis were prepared by dissolving known amounts of substance at room temperature (DL-HPA) or at 60 °C (L-HPA) followed by stagnant evaporation of solvent at room conditions under a fume hood. Employed beakers were covered by perforated sealing films. Crystals obtained were inspected employing a VHX-2000 (Keyence, Japan) microscope with a VH-Z100UR/W objective prior to single crystal analysis. SC-XRD measurement data were collected on a XtaLAB Synergy (Rigaku, Japan), using graphite-monochromated CuKα radiation (λ = 1.54184 Å). Structures were solved by direct methods and all non-hydrogen atoms were refined anisotropically on F^2 (program SHELXTL-97, G.M. Sheldrick, University of Göttingen, Germany). All H atoms were positioned geometrically and refined as riding atoms.

Differential scanning calorimetry and hot stage microscopy. Solid state behavior of DL-HPA was investigated using DSC and HSM. DSC analysis was conducted with a DSC 131 (Setaram Instruments, France) under helium atmosphere. Calibration of the DSC device was regularly performed utilising high-purity indium, tin, zinc and lead. Approximately 8 to 10 mg of DL-HPA received from solubility experiments were weighed into aluminum crucibles, which were then closed. The samples were heated to 400 °C with a heating rate of 2 K min^{-1} followed by a cooling ramp back to room temperature. Only the heating step was evaluated. To support the interpretation of measured DSC curves, hot stage microscopy was conducted using a LTS420 hot stage (Linkam Scientific Instruments, United Kingdom) attached to an Axioskop 2 with Axiocam305 colour camera (Zeiss, Germany). The sample was put onto an object slide and covered by a glass cover. Then, the sample was heated to 400 °C with 10 K min^{-1}, and cooled down to 30 °C after a holding period of 3 min. Prior to HSM, the sample was purified by dissolving a known amount of DL-HPA in water at elevated temperature and recrystallising it by cooling.

3 Results & discussion

3.1 Solid state characterisation of DL-HPA

No PXRD patterns of D-HPA and DL-HPA were found in literature, however L-HPA patterns were reported in our previous work.[11] Therefore, purchased solid phases were analysed by PXRD to enable phase identification of the solids obtained in the SLE experiments. In Fig. 1, PXRD patterns of supplied substances are compared to diffractograms from recrystallised samples or samples from SLE experiments, and a good agreement is found.

The thermal behaviour of L-HPA was described in ref. 11, and the same behaviour is expected for D-HPA based on their identical crystal lattice. A racemic (1 : 1) compound has a different crystal lattice than its corresponding pure enantiomers (here: L- and D-HPA), thus a different thermal behaviour and PXRD pattern are expected. As seen in Fig. 1, the measured diffractograms of D and L-HPA are identical, while the DL-HPA pattern looks similar but is shifted to lower 2θ angles and more reflexes are visible *e.g.* in the 2θ range between 18° and 28°. In DSC measurements, Fig. 2, DL-HPA undergoes a strong endothermic event starting at around 246 °C and an onset temperature of 284 °C. Surprisingly, in ref. 12 the melting point of DL-HPA was reported as greater than 300 °C and no other thermal events were mentioned. Further, the employed measurement method was not explained and

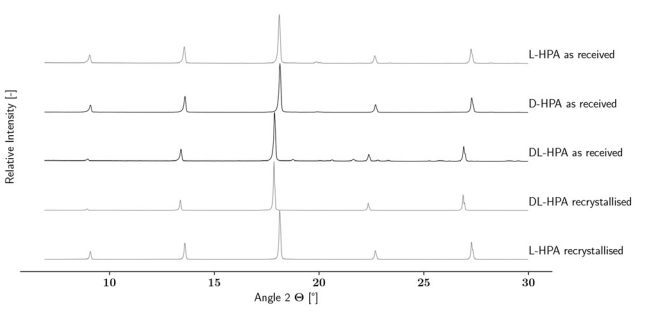

Fig. 1 PXRD patterns of L-HPA, D-HPA and DL-HPA as received and after recrystallisation. Note that L-HPA and D-HPA have identical PXRD patterns.

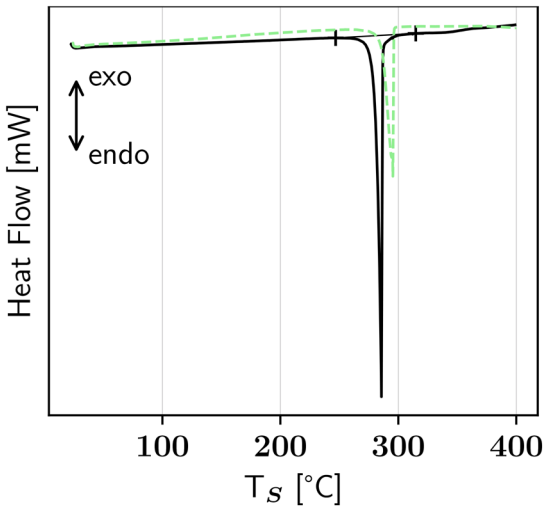

Fig. 2 Measured DSC curve of DL-HPA (solid black line) in comparison to L-HPA from ref. 11 (dashed green line). Start and end temperatures of the DL-HPA thermal event are marked by crosses.

thus the lower temperature event might have been overlooked.† In the safety data sheets, either a melting temperature of 294 °C (ref. 13) or a decomposition at 282 °C (ref. 14) is provided, making available literature data heterogeneous. However, HSM (Fig. 3) reveals first crystals start to move at around 201 °C, followed by disappearance and transformation to liquid-appearing droplets at temperatures higher than approximately 210 °C. The movement of the respective crystals might be caused by formation of gases *e.g.* from decomposition or sublimation. The colour of these droplets changes to dark brown with increasing temperature and is clearly visible at temperatures higher than 240 °C. After cooling to 30 °C, no recrystallisation was encountered. This indicates that the large sharp endothermic event in the DSC measurements does not correspond to single melting, but rather a combined melting decomposition-dominated process. This result is supported by the measured enthalpic value of the related peak of ≈145 ± 4 kJ mol^{-1} (Table S1), which significantly exceeds the usual range of melting enthalpies for amino acids of ≈20 to 60 kJ mol^{-1} determined *via* fast scanning calorimetry.[19] Note, that some crystalline-appearing solid remained after the heating run in HSM in Fig. 3f. The temperature deviation between the decomposition peak in DSC and visible decomposition in HSM could be attributed to an elevated heating rate and different conditions: in DSC the sample is located as a pile in a closed crucible while in HSM the sample is spread as a thin layer between glass plates. Therefore, the particle surface in contact with the set temperature is greater and the heat transfer could be faster.

† The described substance is called DL-HPA but the assigned number corresponds to an intermediate in ref. 12.

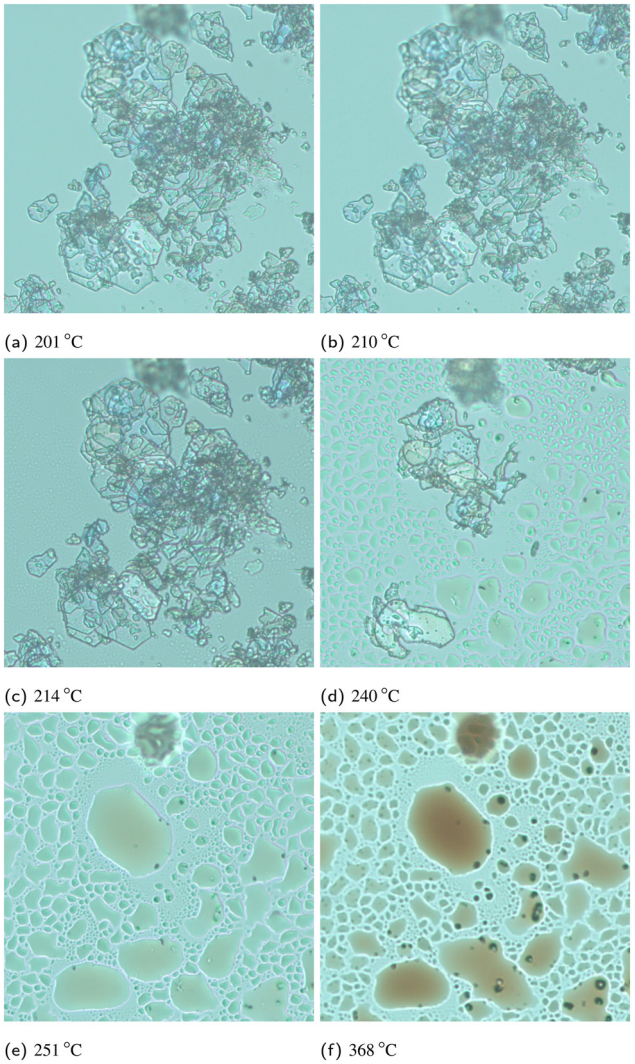

Fig. 3 Selected zoomed pictures of HSM analysis of DL-HPA. The respective sample was recrystallised with agitation.

Although a cover glass was used in HSM, air might still come into contact with the sample providing oxygen for (partial) oxidation which could begin at lower temperatures compared to thermal decomposition in DSC measurements. Residual air in the DSC crucible might facilitate partial oxidation as well, but the supply is limited due to employed sweeping gas. This could explain why a kinetically limited decomposition/oxidation might be visible in HSM prior to the DSC measurement. A decomposition prior to melting is usual for amino acids[1,19] and DL-HPA, as well as L-HPA follow this behaviour. The general thermal behaviour of DL-HPA is similar to L-HPA, see Fig. 2, but slightly different temperatures for the respective events were observed. The endothermic event of L-HPA has an onset of ≈292 °C,[11] while the onset of DL-HPA is 284 °C. Thermogravimetric analysis for L-HPA was performed in literature[11] and significant mass loss at elevated temperature was observed. Due to comparable DSC and HSM results, a similar behaviour in thermogravimetric analysis is expected for DL-HPA.

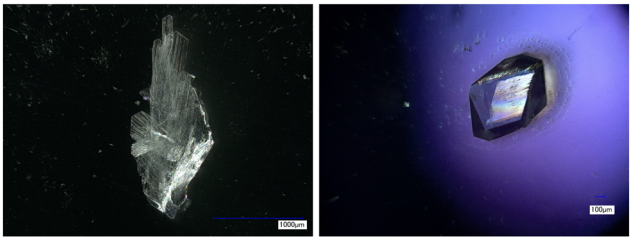

(a) L-HPA (b) DL-HPA

Fig. 4 Microscopic pictures of recrystallised L-HPA and DL-HPA crystals without applying agitation.

Samples recrystallised by stagnant evaporation without agitation were also investigated under the microscope, as shown in Fig. 4. Significant changes of the crystal shape between L-HPA and DL-HPA were encountered. L-HPA crystallised as flat (plate-like) needles while DL-HPA crystals are more spherical, indicating a different crystal morphology. Note that the DL-HPA crystals in Fig. 3 appear more plate-like than in Fig. 4b, which could be attributed to the different recrystallisation techniques used.

3.2 Structure determination of L- and DL-HPA crystals

Crystallographic data and processing parameters of L-HPA and DL-HPA are summarised in Table 2, and molecular structures in the solid state are visualised in Fig. 5(a) and (b), respectively. L-HPA crystallises in the monoclinic space group $P2_1/c$, DL-HPA in the triclinic space group $P1$. The X-ray structure analysis shows that the L-form is present in the crystal structure of L-HPA and the D-form is additionally present in the DL-HPA crystal. The unit cell constants of the two crystal structures are comparable, with two shorter and one longer cell constant. Both the L- and DL-forms are composed of a two-layer system with a hydrogen bonding layer of $-NH_3-$ and –COO– groups of neighbouring molecules. Structure data are deposited in the Cambridge Crystallographic Data Centre (CCDC) under the deposition numbers 2463661 and 2463662.

Table 2 Crystallographic data of L-HPA and DL-HPA unit cells

	L-HPA	DL-HPA
Crystal system	Monoclinic	Triclinic
Space group	$P2_1/c$	$P1$
a [Å]	20.2865(5)	5.4103(1)
b [Å]	4.8114(1)	9.0720(2)
c [Å]	9.8103(2)	19.9535(5)
α [°]	90	78.241(2)
β [°]	102.994(2)	84.522(2)
γ [°]	90	86.777(2)
V [Å^3]	933.03(4)	953.75(4)
Z	4	4
Reflections collected	6111	10 706
Independent reflections	1789	4729
Parameter	118	554
R^1 $[I > 2\sigma_I]$	0.0425	0.0656

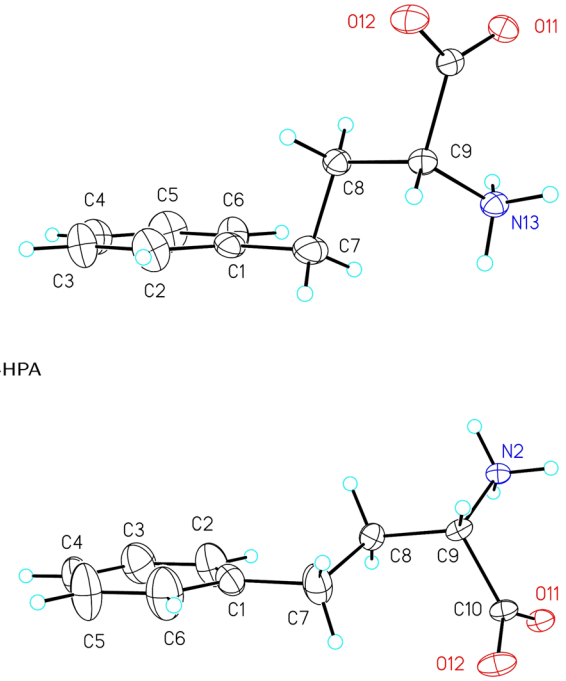

Fig. 5 Single molecules in the crystal structure of L-HPA (a) and DL-HPA (b).

The obtained structures of L-HPA and DL-HPA were employed for calculation of the respective diffractogram with Mercury 2022.2.0 Build 353591 (CCDC, United Kingdom) and compared to measured patterns (phases as received) in Fig. 6. All peaks measured in the recrystallised sample of DL-HPA are well pronounced in the sample as received indicating the same solid phase. Additional less pronounced peaks in the DL-HPA sample as received correlate well to reflexes in the calculated pattern. The crystal structure was determined from recrystallised sample making it unlikely that the additional peaks are caused by

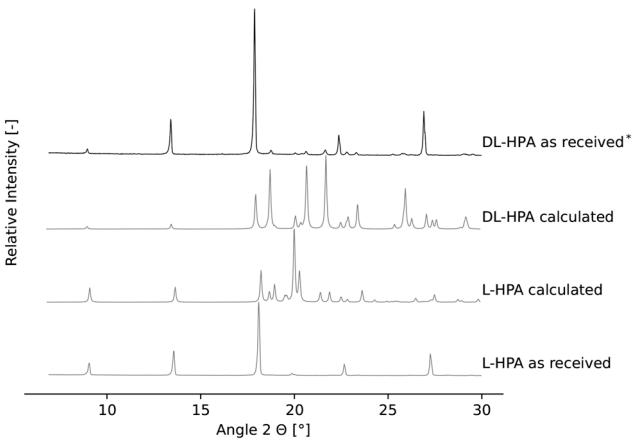

Fig. 6 PXRD patterns of calculated and measured L-HPA and DL-HPA samples. The relative intensity of the pattern marked with * was multiplied by the factor two to improve clarity.

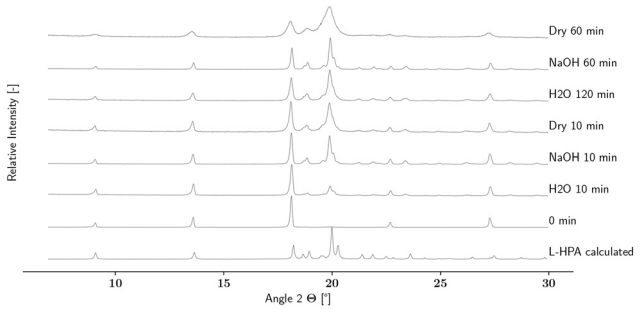

Fig. 7 PXRD patterns of calculated, dry milled, and liquid-assisted milled L-HPA samples.

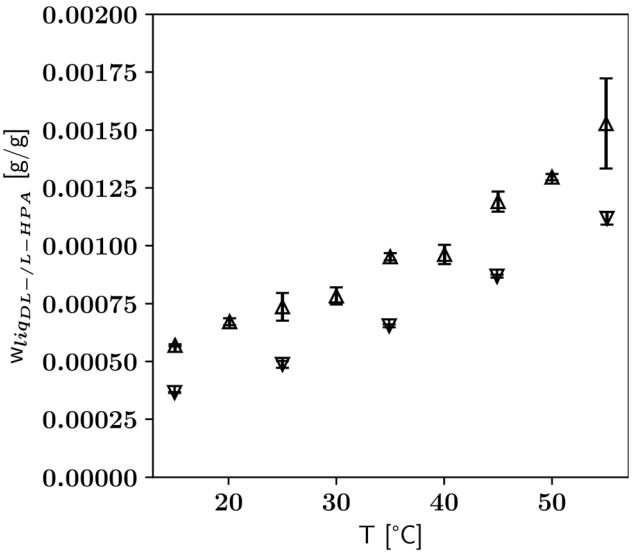

Fig. 8 Solubility of DL-HPA (▽) in water as a function of temperature in comparison to the solubility data of L-HPA (△) taken from literature.[11] Error bars according to the standard deviation of the population.

impurities. Therefore, we conclude that all three DL-HPA patterns correspond to the same solid phase and differences between the patterns are caused by crystal shape and size of our samples. This is even more striking for the L-HPA case and was therefore investigated.

As discussed before, L-HPA exhibits a flat plate to needle-like crystal shape, which led to the hypothesis of a preferred orientation of L-HPA crystals on the employed sample holder, where small surfaces of the respective crystals might not be detected resulting in missing peaks in the powder pattern. To evaluate this hypothesis, milling experiments (both dry and wet, see Section 2.3) were performed to harmonise the edge lengths of the crystals and therewith avoiding preferred orientation. The respective diffractograms are shown in in Fig. 7.

The diffractogram without milling (0 min), shows only 7 well pronounced reflexes while the calculated pattern contains significantly more. At a milling time of 10 min most of the peaks from the calculated pattern are now well visible. At 60 min the formerly not detected peaks increased in intensity which can be nicely illustrated with the peaks at 18°, 19°, and 20°. In the starting pattern, only the peak at 18° is visible, at 10 min the reflexes have the same relative intensity. The peak at 20° is nearly invisible at 0 min and has a highest intensity after 60 min in all investigated cases. In all milling experiments, only the same L-HPA solid phase was detected also in presence of NaOH solution. Liquid-assisted grinding seems to promote sharper reflexes, especially for NaOH solution. Dry milling results in peak broadening due to small crystals and potentially amorphous solid content, rendering the detection of small peaks challenging. A transformation of employed crystals to a different crystalline phase by the application of energy in the milling step would favour potential metastable phases over stable equilibrium ones, which was not observed. Based on results obtained, we conclude that the solid phases taken from our experiments and the determined structure are the same and differences in measured diffractograms can be attributed to preferred orientation of the samples on the sample holder of the PXRD device.

3.3 SLE of D-HPA/L-HPA/water system

SLE data were obtained *via* an isothermal method as described in Section 2.2 and will be presented in this section. The solubilities of DL-HPA and L-HPA in water are visualised as a function of temperature in Fig. 8. Both are relatively low for an amino acid, with around 0.037 wt% at 15 °C and 0.112 wt% at 55 °C for DL-HPA, which even falls below the solubility of L-HPA. DL-HPA was verified as thermodynamically stable phase, and the obtained PXRD patterns fit well to the patterns in Fig. 1.

The respective phase diagram for the aqueous L-HPA/D-HPA chiral system is plotted in Fig. 9b together with a scheme of an intermediate compound forming system in Fig. 9a. As seen, the system is clearly of intermediate compound forming character with eutectic compositions close to the enantiomers side. Experiments using L-HPA and DL-HPA as starting materials gave comparable results as those employing L-HPA and D-HPA. Fig. S1 and S2 show selected PXRD patterns of solids obtained in the equilibration experiments and the respective phase identity is also illustrated in Fig. 9b. For pure L-HPA (100 wt% L-HPA) in the solid at 25 °C, only the reference pattern of L-HPA was found. With decreasing L-HPA content from 96.8 wt% to 57.3 wt% the measured patterns indicate the presence of a mechanical mixture of L-HPA and DL-HPA crystals in equilibrium with liquid of eutectic composition. Between 52.2 wt% and 49.7 wt%, only the DL-HPA X-ray pattern was found, while from 40.8 wt% to 13.7 wt% again a mechanical mixture of DL-HPA and D-HPA was proven. For pure D-HPA (0 wt% L-HPA), only the reference pattern of L-HPA/D-HPA was measured. Therefore, L-HPA was assigned to patterns with L-HPA solid contents of more than 50 wt%, and D-HPA for compositions with less than 50 wt%. At 55 °C (Fig. S2) a similar behaviour with changed L-HPA contents in the solid can be seen. Some samples between 53.3 and 50.6 wt% L-HPA, show a mechanical mixture between L-HPA or D-HPA and DL-HPA, where only the DL-HPA pattern is expected. We hypothesise that some crystals of D-HPA or L-HPA could have remained unnoticed in the solution prior to equilibration period in those samples. Besides nucleation and

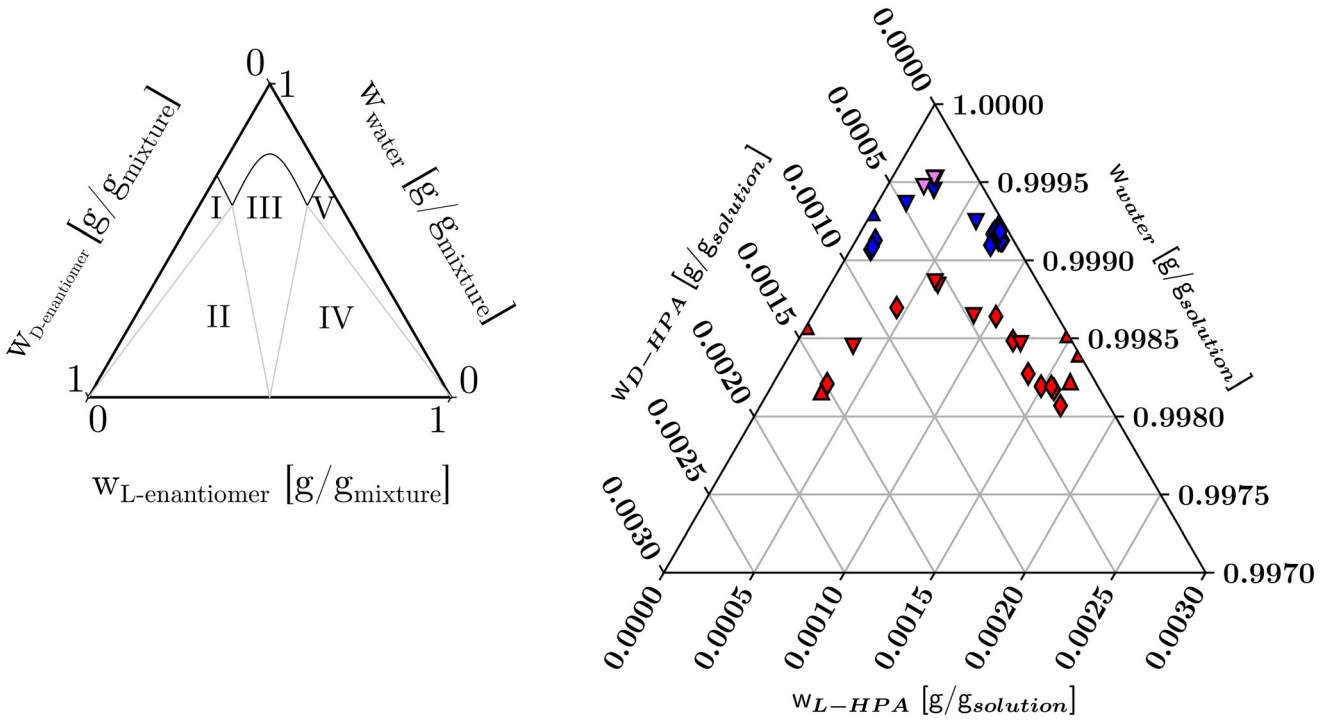

(a) Sketch of a racemic compound forming system. (b) Ternary phase diagram of the L-HPA / D-HPA/ water.

Fig. 9 Sketch of a racemic compound forming system (a) and obtained ternary phase diagram in the L-HPA/D-HPA/water system (b) at 25 °C (blue) and 55 °C (red). Areas I to V in (a) correspond schematically to sections in the Roozeboom diagram, Fig. 10. Symbols in (b) represent the identity of equilibrated solid phase(s): L-HPA: ▲, DL-HPA: ▼, L-HPA or D-HPA + DL-HPA: ♦. Violet symbols refer to the test for the thermodynamically stable phase.

growth of new DL-HPA crystals, the growth of the remained seed crystals would occur. This behaviour was only observed at 55 °C and not in the 25 °C experiments and we attribute that to the ratio between nucleation and growth kinetics. The supersaturation in 25 °C samples is greater than for the 55 °C samples and therefore primary nucleation is favoured. This results in more crystals especially of the thermodynamically stable form, reducing the influence of potentially remained seed crystals on the measured diffractograms. Data from the test on the thermodynamically stable solid phase (see Section 2.2) are shown in Fig. 9b and align well with data from the ternary SLE experiments. This indicates, that DL-HPA is in fact the thermodynamically stable phase and that potentially remained seed crystals did not influence the SLE significantly at 25 °C.

To further clarify the solid-state behaviour, distribution or so called Roozeboom diagrams, can be employed. These visualize the solvent-free compositions of the liquid (eqn (1)) and the equilibrated solid phase and allow visual identification of respective SLE behaviour.[20,21]

$$w^*_{\mathrm{liq,L-HPA}} = \frac{w_{\mathrm{liq,L-HPA}}}{w_{\mathrm{liq,L-HPA}} + w_{\mathrm{liq,D-HPA}}} \quad (1)$$

In Fig. 10, the diagram is plotted for the investigated L-HPA/D-HPA/water system. The vertical axis illustrates the solvent-free L-HPA content in the liquid, while the horizontal shows the L-HPA content in the solid. From left to right five segments are sketched by the lines and symbols:

I Vertical section in which varying liquid compositions are in equilibrium with a pure solid phase, where only D-HPA was found in PXRD.

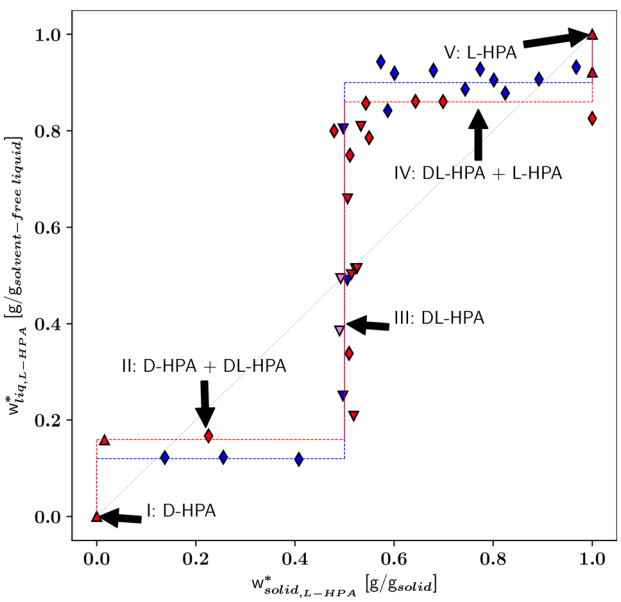

Fig. 10 Distribution diagram of the aqueous chiral HPA system with the solvent-free liquid and solid phase compositions at 25 °C (blue) and 55 °C (red) with the test on the thermodynamically stable phase (violet) at 25 °C. Symbols represent the identity of equilibrated solid phase: L-HPA or D-HPA: ▲, DL-HPA: ▼, L-HPA or D-HPA + DL-HPA: ♦.

Table 3 Solvent-free eutectic compositions and respective water contents

T [°C]	$w^*_{liq,L-HPA,max,1}$ [g/g$_{solvent\text{-}free\ liquid}$]	$w_{liq,H_2O,max,1}$ [wt%]	$w^*_{liq,L-HPA,max,2}$ [g/g$_{solvent\text{-}free\ liquid}$]	$w_{liq,H_2O,max,2}$ [wt%]
25	≈0.12	≈99.91	≈0.91	≈99.92
55	≈0.16	≈99.82	≈0.83	≈99.82

II Horizontal section, where one fixed liquid composition is in equilibrium with two distinct solid phases in varying ratio. Here D-HPA and DL-HPA patterns were encountered in PXRD.

III Vertical section, where varying liquid compositions are in equilibrium with pure DL-HPA crystals.

IV Horizontal line with one fixed liquid composition in equilibrium with L-HPA and DL-HPA solid phases in varying ratio.

V Vertical section with varying liquid compositions in equilibrium with pure L-HPA crystals.

Our obtained plot follows the behaviour of a 1:1 intermediate compound or cocrystal. Such a system has a specific fixed 1:1 composition in the solid state in equilibrium with varying liquid compositions and therefore results in a vertical line in the Roozeboom plot.[21] For a chiral system, this 1:1 composition marks the racemic one, thus confirming the racemic compound forming type of system for the studied D-HPA/L-HPA case. This hypothesis is further supported by the characteristic shape[22] of the liquidus line in Fig. 9b. The system behaves approximately symmetrical as has been shown with a few samples with a solvent-free mass fraction of D-HPA higher than 0.5. Deviations from the perfect symmetry could originate from inaccuracies of HPLC measurements due to low concentrations. Further, the solubility maxima compositions, specifying the eutectic compositions in the chiral system in Fig. 9b and reported in Table 3, vary with temperature. Such changes can be exploited for separation.[23,24]

3.4 Comparison to phenylalanine

While literature data for the synthetic α-amino acid HPA are very scarce, the structurally similar phenylalanine (PHE) is well investigated. Both compounds only differ in the presence/absence of a –CH_2– group in the aliphate carbon chain as can be seen in Fig. 11. The solid-state behaviour of L-PHE was studied frequently and two anhydrous polymorphs, a hemihydrate, and a monohydrate[25–30] are known. In our investigations of L-HPA,[11] no evidence for polymorphism or hydrates were observed. For the thermal behaviour of anhydrous L-PHE, three endothermic events were detected at 262, 277, 292 °C in ref. 25 and at 255, 275, and 290 °C in ref. 31. In both works, a heating rate of 10 min^{-1} was employed and in ref. 25, simultaneous melting and decomposition was detected, while surprisingly, in ref. 31 a melting behaviour of the substance was claimed. This correlates well to the temperature of the large endothermic event reported at 277 °C in ref. 32. In ref. 19, a strong sublimation or evaporation of L-PHE was observed and the melting point was obtained using fast scanning calorimetry with a heating rate of several thousand K s^{-1} at 306 ± 7 °C. For L-HPA, we found one large endothermic event at around 292 °C with 2 K min^{-1} and hypothesised a (partial) decomposition.[11] DL-PHE crystals grown in sodium metasilicate gel were investigated in ref. 33 finding several decomposition steps starting at around 210 °C with a heating rate of 10 K min^{-1}. Interestingly, in ref. 27, the growth of a racemic crystal of PHE is assessed as unlikely from aqueous solution with formic or acetic acid. For DL-HPA we observed mainly decomposition with an onset of 284 °C in DSC measurements compared to decomposition of DL-HPA at 282 °C reported in the material safety data sheet.[14]

Solubilities of L-PHE and DL-PHE were investigated several times in water and aqueous mixtures.[25,29,31,32,34–38] The solubility of the enantiomers of PHE is much higher than that of HPA (≈30 times for DL-form, ≈40 times for the L enantiomer at 25 °C), which could be attributed to the increased chain length of the HPA molecule (see Fig. 11).[39] In both cases, the measured solubility of the (anhydrous) L-form exceeds the solubilities determined for the respective DL-form. Both systems form racemic compounds and the eutectic compositions in the aqueous chiral PHE system at 25 °C are found at solvent-free mass fractions of L-PHE of around 8 and 92 wt%,[40] in comparison to values around 12 and 91 wt% L-HPA in the L-HPA/D-HPA/water system. While structures and PXRD patterns of L-PHE solid phases are available,[26–28] no diffractogram for DL-PHE was reported to the best of our knowledge. Two old entries for DL-PHE crystal structures were found in the CCDC (QQQASG and QQQASG01) where a 3D structure was unavailable. Therefore, no comparison to DL-HPA was feasible. When comparing the crystal structures of D-PHE (EQUYEX) and L-PHE (QQQAUJ13), it is noteworthy that the Z' = 4 observed at 2 occurs in both D-PHE and L-PHE. The isomers of PHE also arrange themselves in the same way as in L-HPA and DL-HPA crystals, forming a two-layer system with a hydrogen bonding layer. In contrast to the crystal structures of L-HPA and DL-HPA, the

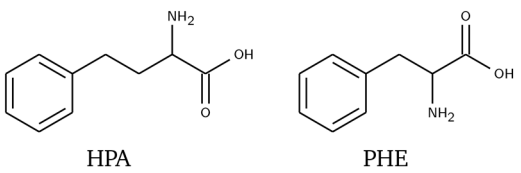

Fig. 11 Structures of HPA and PHE.

layer spacing of the two isomers of PHE with N···N: L-PHE: 3.675 Å, D-PHE: 3.559 Å, is significantly shorter than with L-HPA: N···N 4.753 Å and DL-HPA: 4.101 Å.

4 Conclusions

In this work, the thermal stability behaviour of DL-HPA was investigated *via* DSC and HSM showing a decomposition-dominated thermal behavior with an peak onset of 284 °C. Thus, no melting point can be reported. Determined solubility of DL-HPA is extraordinary low with 0.037 wt% at 15 °C and increases with temperature to 0.112 wt% at 55 °C. Our study regarding the thermodynamically stable solid phase at racemic composition indicated the DL-HPA compound as the stable phase at 25 °C. The ternary phase diagram of the aqueous chiral HPA system demonstrated the system to exhibit intermediate compound forming behaviour with DL-HPA as the (racemic) 1 : 1 compound of D-HPA and L-HPA. The solvent-free eutectic compositions at 25 °C and 55 °C were verified at L-HPA concentrations of ≈12 wt% and ≈91 wt% and ≈16 wt% and ≈83 wt%, respectively. Thus, pure enantiomer can be crystallized directly from solution at compositions below or above these values, *i.e.* D- or L-HPA, respectively. Kinetic preferential crystallization might be utilized also in-between these compositions. However, the racemic compound, that is the racemic composition, is still the limiting factor for purification. Observed deviations from the perfect symmetry could be caused by analytical challenges. Although some L-HPA or D-HPA was proven in concentration ranges where only DL-HPA was expected at 55 °C, the liquidus line follows the typical shape for this kind of systems and the influence from the L-HPA or D-HPA crystals seems to be negligible. Single crystal structures were determined from L-HPA and DL-HPA crystals produced by stagnant evaporation. When comparing X-ray powder patterns calculated from the L-HPA structure with diffractograms obtained from equilibration experiments, in the latter only some reflexes of the L-HPA were well pronounced due to preferred crystal orientation. By milling experiments we were able to bring experimental patterns in agreement with the calculated one, suggesting a strong influence of preferred orientation on measured PXRD patterns. Considering the comparison between the chiral PHE and HPA systems, we conclude that both systems have a similar thermal behaviour and their SLE behaviour in water partly aligns *e.g.* with regard to the eutectic compositions, but with strongly increased solubilities in the PHE system. Altough we found no evidence of hydrate or polymorphic forms of L-HPA or DL-HPA under the conditions used new solid forms might be revealed by further investigation as it was the case for L-PHE.

The presented work was challenging due to extremely low solubilities of HPA, L-HPA crystals which showed floating behaviour on water, and very similar measured L- and DL-HPA PXRD patterns influenced by preferred orientation of the respective crystals. Further research could be focused on the extension of data obtained in this work, *e.g.* by covering a greater temperature range for solubilities. Our experiments could be further validated by refined experimental methods, which rule out the presence of seed crystals in the samples prior to cooling. Further, the thermal behaviour of DL-HPA is not completely clear yet, for example the identity of the decomposition products that might be of interest. The melting point of DL-HPA could potentially be revealed by more specialized measurement methods such as fast scanning calorimetry.[19]

Author contributions

Axel Schultheis: conceptualization, methodology, validation, formal analysis, investigation, data curation, writing – original draft, writing – review & editing, visualization. Klaus Merz: methodology, investigation, data curation, writing – original draft, writing – review & editing, visualization. Vico Tenberg: conceptualization, methodology, formal analysis, writing – review & editing, supervision. Heike Lorenz: conceptualization, resources, writing – review & editing, supervision, project administration, funding acquisition.

Conflicts of interest

There are no conflicts to declare.

Data availability

The supporting data has been provided as part of the supplementary information (SI). Table S1: measured enthalpies of endothermic effects in the DSC analysis of DL-HPA, Table S2: measured individual data points in binary SLE determination of DL-HPA, Table S3: averaged measured data points in binary SLE determination of DL-HPA, Table S4: details on the test on the stable phase in the chiral system at 25 °C, Table S5: SLE data in the D-HPA/L-HPA/water system. Fig. S1 and S2 illustrate PXRD data of the solids obtained in the SLE determination in the D-HPA/L-HPA/water system.

Supplementary information is available. See DOI: https://doi.org/10.1039/d6ce00109b.

CCDC 2463661 and 2463662 contain the supplementary crystallographic data for this paper.[41a,b]

Acknowledgements

The authors would like to thank Jacqueline Kaufmann and Stefanie Oberländer for their continuous assistance in the lab, especially for their support in HPLC and PXRD measurements. Additional support in labwork by Carmen Albers is greatly acknowledged by the authors. The Project is funded by the Deutsche Forschungsgemeinschaft (DFG, German Research Foundation) – 501735683, gefördert durch die Deutsche Forschungsgemeinschaft (DFG) – 501735683. The authors gratefully acknowledge the funding by the European Regional Development Fund (ERDF) within the programme Research and Innovation – Grant Number ZS/2023/12/182075 supporting Vico

Tenberg in his work. Open Access funding provided by the Max Planck Society.

References

1 V. Ahluwalia, L. S. Kumar and S. Kumar, *Chemistry of Natural Products: Amino Acids, Peptides, Proteins and Enzymes*, Springer International Publishing, 2022.
2 H. Lorenz and A. Seidel-Morgenstern, *Angew. Chem., Int. Ed.*, 2014, **53**, 1218–1250.
3 *Chiral Separations*, ed. D. Stevenson and I. D. Wilson, Springer US, 1988.
4 *Molecular Mixed Crystals*, ed. M. Àngel Cuevas-Diarte and H. A. J. Oonk, Springer International Publishing, 2021.
5 *Novel Optical Resolution Technologies*, ed. K. Sakai, N. Hirayama and R. Tamura, Springer Berlin Heidelberg, 2007.
6 J. Gänsch, K. Oliynyk, S. Potharaju, A. Seidel-Morgenstern and H. Lorenz, *Ind. Eng. Chem. Res.*, 2024, **63**, 18525–18535.
7 E. Schmidt, O. Ghisalba, D. Gygax and G. Sedelmeier, *J. Biotechnol.*, 1992, **24**, 315–327.
8 A. L. Ahmad, P. C. Oh and S. R. A. Shukor, *Biotechnol. Adv.*, 2009, **27**, 286–296.
9 B.-K. Cho, J.-H. Seo, J. Kim, C.-S. Lee and B.-G. Kim, *Biotechnol. Bioprocess.*, 2006, **11**, 299–305.
10 E. Heuson, F. Charmantray, J.-L. Petit, V. de Berardinis and T. Gefflaut, *Adv. Synth. Catal.*, 2019, **361**, 778–785.
11 V. Tenberg, M. Sadeghi, A. Schultheis, M. Joshi, M. Stein and H. Lorenz, *RSC Adv.*, 2024, 10580–10589.
12 M. F. Oldfield and N. P. Botting, *J. Labelled Compd. Radiopharm.*, 1998, **41**, 29–36.
13 TCI EUROPE N.V., *Safety Data Sheet for DL-Homophenylalanine H1329*, https://www.tcichemicals.com/BE/en/sds/H1329_EU_6N.pdf, 2018, Revision 1, retrieved on 05.06.2025.
14 Sigma-Aldrich Chemie GmbH, *Safety Data Sheet for DL-Homophenylalanine*, https://www.sigmaaldrich.com/DE/en/sds/aldrich/294357?userType=anonymous, 2025, Version 6.7 retrieved on 05.06.2025.
15 Thermo Fisher Scientific Chemicals, Inc., *Safety Data Sheet for D-Homophenylalanine H27629*, https://assets.thermofisher.com/DirectWebViewer/private/document.aspx?prd=ALFAAH27629~~PDF~~MTR~~AGHS~~EN~~2024-03-30%2022:56:27~~D-Homophenylalanine~~, 2024, Revision 3, retrieved on 02.06.2025.
16 V. Tenberg, M. Stein and H. Lorenz, *Crystals*, 2023, **13**, 1542.
17 S. Hsu, H. Lo, C. Kao, D. Lee and W. Hsu, *Biotechnol. Prog.*, 2006, **22**, 1578–1584.
18 S. Verseck, A. Bommarius and M.-R. Kula, *Appl. Microbiol. Biotechnol.*, 2001, **55**, 354–361.
19 H. T. Do, Y. Z. Chua, A. Kumar, D. Pabsch, M. Hallermann, D. Zaitsau, C. Schick and C. Held, *RSC Adv.*, 2020, **10**, 44205–44215.
20 S. W. Lin, K. M. Ng and C. Wibowo, *Comput. Chem. Eng.*, 2008, **32**, 956–970.
21 F. L. Nordstrom, S. S. Mohajerani, B. Linehan and F. Ricci, *Phys. Chem. Chem. Phys.*, 2022, **24**, 26485–26498.
22 H. Lorenz, in *Crystallization: Basic Concepts and Industrial Applications*, ed. W. Beckmann, Wiley, 2013, ch. Solubility and Solution Equilibria in Crystallization, pp. 35–74.
23 H. Kaemmerer, A. Seidel-Morgenstern and H. Lorenz, *Chem. Ing. Tech.*, 2009, **81**, 1955–1965.
24 T. Le Minh, H. Lorenz and A. Seidel-Morgenstern, *Chem. Eng. Technol.*, 2012, **35**, 1003–1008.
25 J. Lu, Q. Lin, Z. Li and S. Rohani, *J. Chem. Eng. Data*, 2012, **57**, 1492–1498.
26 P. A. Williams, C. E. Hughes, A. B. M. Buanz, S. Gaisford and K. D. M. Harris, *J. Phys. Chem. C*, 2013, **117**, 12136–12145.
27 F. S. Ihlefeldt, F. B. Pettersen, A. von Bonin, M. Zawadzka and C. H. Görbitz, *Angew. Chem., Int. Ed.*, 2014, **53**, 13600–13604.
28 K. P. Nartowski, S. M. Ramalhete, P. C. Martin, J. S. Foster, M. Heinrich, M. D. Eddleston, H. R. Green, G. M. Day, Y. Z. Khimyak and G. O. Lloyd, *Cryst. Growth Des.*, 2017, **17**, 4100–4109.
29 Z. Wang, Y. Li, W. Fang, Q. Wang, H. Xiao and L. Dang, *Ind. Eng. Chem. Res.*, 2014, **53**, 521–529.
30 H. M. Cuppen, M. M. H. Smets, A. M. Krieger, J. A. van den Ende, H. Meekes, E. R. H. van Eck and C. H. Görbitz, *Cryst. Growth Des.*, 2019, **19**, 1709–1719.
31 Y. Li, S. Ling, X. Gao, L. Cheng, K. Li and X. Li, *Colloids Surf., A*, 2024, **703**, 135364.
32 J. Lu and J. a. Wang, *Afr. J. Pharm. Pharmacol.*, 2012, **6**, 269–277.
33 E. Ramachandran and S. Natarajan, *Cryst. Res. Technol.*, 2007, **42**, 617–620.
34 S. Roy, *Russ. J. Phys. Chem. A*, 2022, **96**, 1968–1975.
35 X. Zhou, J. Fan, N. Li, Z. Du, H. Ying, J. Wu, J. Xiong and J. Bai, *Fluid Phase Equilib.*, 2012, **316**, 26–33.
36 S. Mondal, S. Roy, S. Ghosh, K. Mahali and B. K. Dolui, *J. Solution Chem.*, 2016, **45**, 1755–1772.
37 A. Hossain, S. Roy, S. Ghosh, S. Mondal and B. K. Dolui, *RSC Adv.*, 2015, **5**, 69839–69847.
38 S. Ghosh, S. Mondal, S. Roy, S. Saha, D. Subba and B. K. Dolui, *J. Mol. Liq.*, 2018, **249**, 659–665.
39 T. Needham, A. Paruta and R. Gerraughty, *J. Pharm. Sci.*, 1971, **60**, 565–567.
40 M. Klussmann, A. J. P. White, A. Armstrong and D. G. Blackmond, *Angew. Chem., Int. Ed.*, 2006, **45**, 7985–7989.
41 (*a*) CCDC 2463661: Experimental Crystal Structure Determination, 2026, DOI: 10.5517/ccdc.csd.cc2npmyy; (*b*) CCDC 2463662: Experimental Crystal Structure Determination, 2026, DOI: 10.5517/ccdc.csd.cc2npmzz.

